PERGAMON

International Journal of Heat and Mass Transfer 45 (2002) 2577–2585

International Journal of HEAT and MASS TRANSFER

www.elsevier.com/locate/ijhmt

Experimental and numerical investigation of circularly lobed nozzle with/without central plug

You-Hong Liu

Department of Engineering Mechanics, Tsinghua University, Beijing 100084, China

Received 5 September 2001

Abstract

The experimental rig was established for the pumping performance investigation of a circularly lobed nozzle with a central plug, and of the same nozzle without a central plug for comparison. Seven different cylindrical mixers were designed to match the circularly lobed nozzle. Results show that the central plug increases the pumping ratio of the secondary mass flow rate to the primary mass flow rate about 60–70% over the same lobed nozzle without a central plug, and the total pressure prior to flow's entry into circularly lobed nozzle increased about 0.8–1.0% over the same lobed nozzle without a central plug. In order to know the mixing process between the primary and the secondary flows, in addition, a numerical procedure was developed to solve the incompressible Navier–Stokes equations in a curvilinear nonorthogonal coordinate. The numerical results show that there are great differences in the thermal mixing process, of the case with a central plug in which the low temperature contour lines in the exit cross-section of cylindrical mixer can reach the central line of the mixer, from the case without a central plug in which the elevated temperature contour lines in the exit cross-section of cylindrical mixer still occupy the central zone of the mixer. This was the fundamental reason why the thermal mixing efficiency of the lobed nozzle with a central plug was much more than that of without a central plug. Lastly, good agreements of temperature and axial velocity component in the exit cross-section of the mixer had been observed between the numerical results and the measured ones.

Keywords: Central plug; Lobe; Nozzle; Pumping performance; Thermal mixing efficiency

1. Introduction

There are two kinds of the lobed nozzle according to the arrangement of lobes: the straightly lobed nozzle, and the circularly lobed nozzle. The pumping characteristic rapid mixing process of straightly lobed nozzle have been studied extensively while that of the circularly lobed nozzle got a little attention. The role of central plug on promoting pumping performance and thermal mixing efficiency between the primary and the secondary flows of the circularly lobed nozzle has not yet been reported.

In this paper, the experimental rig was firstly established for investigating the pumping performance and thermal mixing efficiency of a circularly lobed nozzle with a central plug, and also of the same lobed nozzle without a central plug. The mixing process between the primary and the secondary flows for the cases with and without a central plug were numerically investigated by solving the Navier–Stokes equations.

2. Experimental approaches

An experimental program was established to determine the pumping performance of circularly lobed nozzle with a central plug in a practical ejector system. The pumping performance, defined as the ratio of the entrained secondary mass flow rate to the supplied primary mass flow rate, is measured for both the same ejector system with and without a central plug. The ejector test rig is shown schematically in Fig. 1. A photograph of the rig is found in Fig. 2. It consists of three main components: the primary flow passage, the

E-mail address: baohong@mail.tsinghua.edu.cn (Y.-H. Liu).

0017-9310/02/$ - see front matter
PII: S0017-9310(01)00339-8

Nomenclature

A	exit cross-sectional area
B	inlet constant cross-sectional area
$\mathrm{Cof}(\partial z_i/\partial\xi_k)$	cofactor of $\partial z_i/\partial\xi_k$ in the Jacobian of the transformation $z_i = z_i(\xi_k)$
C_μ	turbulent coefficient
D_{eq}	equivalent diameter
Δh	pressure difference between the flow duct wall static pressure and the atmospheric pressure ($\mathrm{mmH_2O}$)
IX, IZ	grid layer order of X, Z directions, respectively
J	Jacobian of transformation
K	turbulent kinetic
m	mass flow rate
r_{k}	$r,\ i = 1,2$ (i.e., $z_i = z, r$)1, $\ i = 3$(*i.e.*, $z_i = \theta$)
s_Φ	source term of the Φ transport equation
T	absolute temperature
u_i	velocity components in $z_i(\theta, r, z)$ directions, respectively
U_i	contravariant velocity in the ξ_i direction
W	axial velocity
Z, r, θ	axial, radial, and azimuthal directions, respectively
z_i	cylindrical coordinates

Greek symbols

α	flow coefficient
Γ_Φ	diffusion coefficients of the Φ transport equation
ε	modified gas expand coefficient
ς	wave length of lobe
η	thermal mixing efficiency
θ	ratio of the primary flow absolute temperature to the secondary flow absolute temperature, i.e., $T_{\mathrm{p}}/T_{\mathrm{s}}$
λ	ratio of mixer cross-sectional area to lobed nozzle exit area, i.e., $A_{\mathrm{m}}/A_{\mathrm{p}}$
ξ_i	curvilinear coordinates
ρ	density
Φ	dependent variable, pumping ratio of the secondary mass flow rate to the primary mass flow rate, i.e., $\Phi = m_{\mathrm{s}}/m_{\mathrm{p}}$

Subscripts

p	primary flow
s	secondary flow
mix	fully mixing
max	maximum
1	secondary flow passages with inlet diameter of 100 mm
2	secondary flow passages with inlet diameter of 80 mm

Superscript

n	temperature-corrected parameter.

secondary flow passage, and the cylindrical mixing duct. These are described, respectively, as follows.

The primary flow passage begins with a rectangular cross-sectioned duct having bellmouth inlet and locates in a large space. An electrical single-stage centrifugal blower firstly powers the primary airflow. The aviation fuel is sprayed into the primary airflow, and combusts in the combustion chamber. And then the combusted gas flow of elevated temperature is stabilized in a stable chamber to establish a uniform swirl-free velocity profile prior to the flow's entry into a circularly lobed nozzle. The total temperature and total pressure of the primary flow are determined in the nearly exit cross-section of the stable room with a thermopair and a probe, respectively.

The secondary flow passage is also provided by a pair of round cross-sectioned ducts having bellmouth inlets and locates in a large space. One duct is mounted in a vertical plane, of which the diameter is 100 mm (represented by D100) and the other in a horizontal plane, of which the diameter is 80 mm (represented by D80). The duct inlets are located where it is some distance away from the primary flow passage centerline to reduce disturbance to the entrained chamber air. Entering perpendicular to the primary flow passage centerline, the entrained flow is then turned in the entrained chamber to merge parallel to the centerline. The secondary flow passage area is adjustable by fully plugging one of the two-bellmouth inlets.

The geometry of mixing duct (called as mixer) is in a cylindrical form with axial length equal to diameter. The primary and the secondary flows enter this duct and mix together prior to flowing into ambient air. The total temperatures of mixing flow were determined by a rake in the exit cross-section of the mixer, consisting of seven probes equally spaced across the mixer diameter. The axial velocity of mixing flow in the exit cross-section of the mixer was measured by seven-hole probe equipment.

The test rig permits three parameters to be investigated:

(1) $\lambda = A_{\mathrm{m}}/A_{\mathrm{p}}$,
(2) $A_{\mathrm{s}}/A_{\mathrm{p}}$,
(3) $\theta = T_{\mathrm{p}}/T_{\mathrm{s}}$.

It is possible to vary a particular parameter independently of the other parameters and to carry tests with and without a central plug, respectively.

The primary and the secondary mass flow rates were computed from static pressure measurements in the

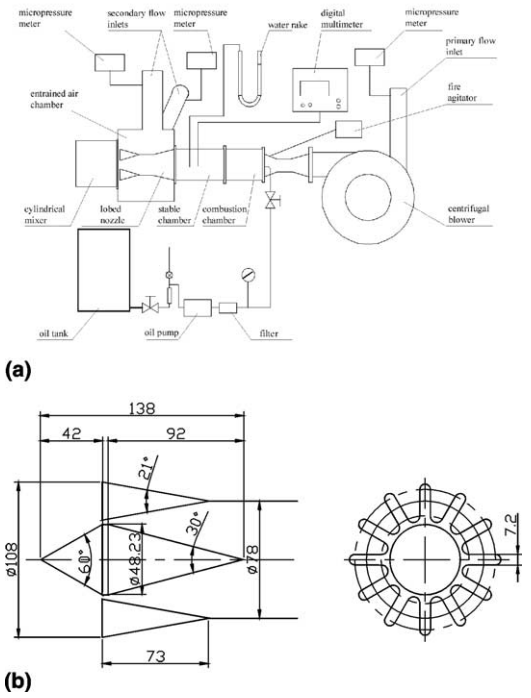

Fig. 1. Experimental rig and drawing of lobed nozzle with central plug.

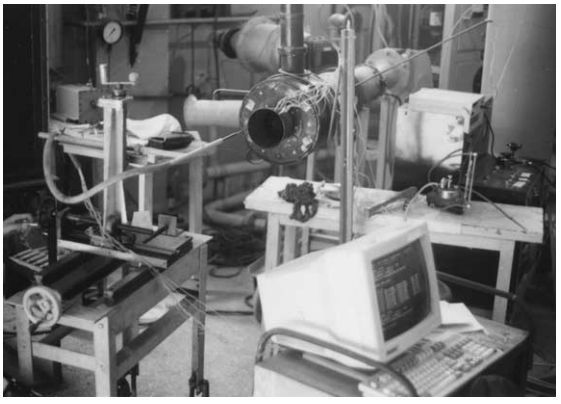

Fig. 2. A photograph of test rig.

constant area inlet portion of the respective flow passage, and is determined by

$$m_{\mathrm{p}} = 0.01594 \times \alpha\varepsilon \times B_{\mathrm{p}} \times \sqrt{\rho \Delta h_{\mathrm{p}}}/3600 = 0.111121725 \times \sqrt{\rho \Delta h_{\mathrm{p}}}, \quad (1)$$

where $\alpha\varepsilon$ is equal to 0.99.

The secondary mass flow rate is determined as

$$m_{\mathrm{s1}} = 0.01594 \times \alpha\varepsilon \times B_{\mathrm{s1}} \times \sqrt{\rho \Delta h_{\mathrm{s1}}}/3600 = 0.03374281 \times \sqrt{\rho \Delta h_{\mathrm{s1}}}, \quad (2)$$

$$m_{\mathrm{s2}} = 0.01594 \times \alpha\varepsilon \times B_{\mathrm{s2}} \times \sqrt{\rho \Delta h_{\mathrm{s2}}}/3600 = 0.02203387 \times \sqrt{\rho \Delta h_{\mathrm{s2}}}. \quad (3)$$

3. Experimental results with and without a central plug

3.1. Temperature-corrected parameter

Presz et al. [1] concluded from ideal gas assumption that if the flow parameter was chosen as $(m_{\mathrm{s}}/m_{\mathrm{p}})(T_{\mathrm{os}}/T_{\mathrm{op}})^{1/2}$ with fixed ejector pressures, the pumping solution would be a function of ejector geometry only. It was seen to correlate reasonably the experimental data into a single pumping curve. In this way, density or temperature effects dropped out of the problem. This allows one to run cold flow tests and to relate the results to more realistic hot flow ejectors. Because the flow parameter was derived from ideal gas assumption, the flow parameter can be replaced by the following temperature-corrected pumping ratio:

$$\Phi' = (m_{\mathrm{s}}/m_{\mathrm{p}})(T_{\mathrm{s}}/T_{\mathrm{p}})^{n} = \Phi\theta^{-n}.$$

Then, the pumping data for all different temperatures would be correlated into a single pumping curve if the temperature-corrected parameter n was equal to 0.4,, as shown in Fig. 3.

3.2. Pumping ratio

Fig. 4 and Table 1 present the comparison of pumping ratio in different temperature of the primary flow, with and without a central plug, for the cylindrical mixer of which the cross-sectional area ratio to lobed nozzle exit area without a central plug is 3.08, and for

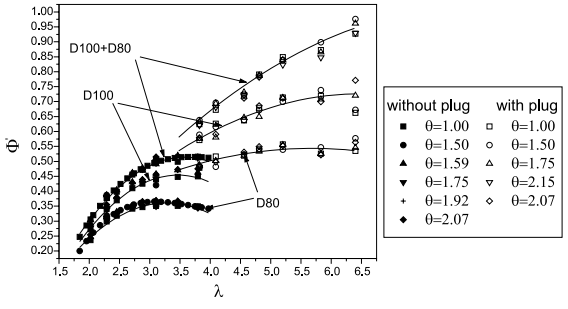

Fig. 3. Temperature-corrected pumping ratio vs area ratio of the mixer to the lobed nozzle with/without central plug.

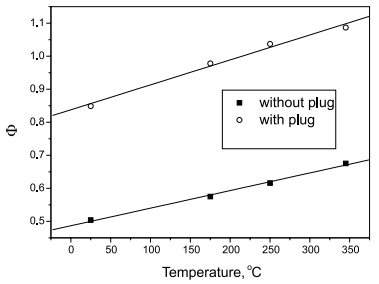

Fig. 4. Pumping ratio vs the primary flow temperature with/without central plug.

Table 1
Pumping ratio in different primary flow temperature

T_p, °C	Without plug, Φ_A	With plug, Φ_B	Φ_B/Φ_A
25	0.5037	0.8491	1.686
175	0.5749	0.9780	1.701
250	0.6159	1.0373	1.684
345	0.6755	1.0869	1.609

the secondary flow inlets of D80 and D100. The pumping ratio with a central plug is increased about 60–70% over that without a central plug in the same test rig. The maximum temperature-corrected pumping ratio without a central plug is 0.54, while it is more than 0.9 with a central plug.

3.3. Total pressure of the primary flow

Fig. 5 and Table 2 present the total pressure of the primary flow prior to flow's entry into lobed nozzle in different primary flow temperature, with and without a central plug. From Table 2, it is seen that the total pressure prior to flow's entry into lobed nozzle with a central plug increases clearly but slightly, as compared to that without a central plug. And the increased value of total pressure is different for different primary flow

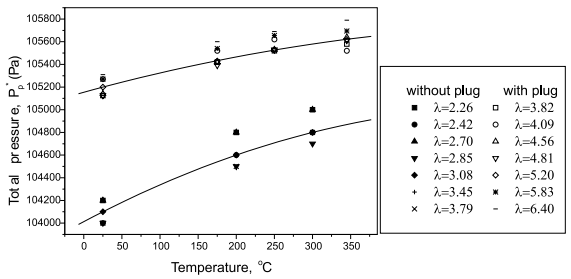

Fig. 5. Total pressure vs main flow temperature.

Table 2
Total pressure prior to flow's entry into lobed nozzle (Pa)

λ	T_p			
	25 °C	200 °C	300 °C	
Without plug				
2.26	104 200	104 800	105 000	
2.42	104 000	104 600	104 800	
2.70	104 200	104 800	105 000	
2.85	104 000	104 500	104 700	
3.08	104 100	104 600	104 800	
3.45	104 100	104 800	105 000	
3.79	104 000	104 500	104 800	
	25 °C	175 °C	250 °C	345 °C
With plug				
3.82	105 130	105 420	105 520	105 580
4.09	105 270	105 520	105 620	105 520
4.56	105 140	105 420	105 530	105 640
4.81	105 130	105 390	105 530	105 610
5.20	105 200	105 430	105 530	105 620
5.83	105 270	105 540	105 660	105 700
6.40	105 310	105 590	105 690	105 790

temperature. The increased value of total pressure with a central plug is about 0.8–1.0% over the same primary flow temperature without a central plug. From the statistical results it is derived that the primary mass flow rate without a central plug would increase to 1.6–1.7 times more than that with a central plug, if the same entrained secondary mass flow rate was desired.

4. Model describing flow field and numerical method

The flow in the lobed nozzle mixer is three-dimensional, incompressible, and turbulent. Since the mixing process actually takes place in the shear layer between the two internal streams, the standard k–ε viscosity model whose empirical constants were found to give good agreement in a wide range of shear flows, models the turbulent flows. For an entity Φ the conservation equation in cylindrical coordinates could be cast into the following form:

$$\frac{1}{r}\left(\frac{\partial}{\partial\theta}(\rho u_1\Phi)+\frac{\partial}{\partial r}(r\rho u_2\Phi)+\frac{\partial}{\partial z}(r\rho u_3\Phi)\right) = \frac{1}{r}\left[\frac{\partial}{\partial\theta}\left(\frac{\Gamma_\Phi}{r}\frac{\partial\Phi}{\partial\theta}\right)+\frac{\partial}{\partial r}\left(r\Gamma_\Phi\frac{\partial\Phi}{\partial r}\right)+\frac{\partial}{\partial z}\left(r\Gamma_\Phi\frac{\partial\Phi}{\partial z}\right)\right]+S_\Phi. \quad (4)$$

To copy with the irregular geometries of the lobed nozzle, a transformation of the coordinate system $z_i(\theta,r,z)$ becomes necessary such that the boundaries are fitted by the curvilinear coordinates $\xi_i(\xi,\eta,\zeta)$. By using

the chain rule to perform the transformation, the above equation can be written as:

$$\frac{1}{\mathrm{Jr}}\left(\frac{\partial(\rho U_1\Phi)}{\partial\xi}+\frac{\partial(\rho U_2\Phi)}{\partial\eta}+\frac{\partial(\rho U_3\Phi)}{\partial\zeta}\right)$$
$$=\frac{1}{\mathrm{Jr}}\left\{\frac{\partial}{\partial\xi}\left[\frac{\Gamma_\Phi}{\mathrm{Jr}}\left(\frac{\partial\Phi}{\partial\xi}B_1^1+\frac{\partial\Phi}{\partial\eta}B_2^1+\frac{\partial\Phi}{\partial\zeta}B_3^1\right)\right]\right.$$
$$+\frac{\partial}{\partial\eta}\left[\frac{\Gamma_\Phi}{\mathrm{Jr}}\left(\frac{\partial\Phi}{\partial\xi}B_1^2+\frac{\partial\Phi}{\partial\eta}B_2^2+\frac{\partial\Phi}{\partial\zeta}B_3^2\right)\right]$$
$$\left.+\frac{\partial}{\partial\zeta}\left[\frac{\Gamma_\Phi}{\mathrm{Jr}}\left(\frac{\partial\Phi}{\partial\xi}B_1^3+\frac{\partial\Phi}{\partial\eta}B_2^3+\frac{\partial\Phi}{\partial\zeta}B_3^3\right)\right]\right\}+S_\Phi, \quad (5)$$

where

$$U_1=(z_\eta r_\zeta-z_\zeta r_\eta)u_1+r(\theta_\eta z_\zeta-\theta_\zeta z_\eta)u_2+r(r_\eta\theta_\zeta-r_\zeta\theta_\eta)u_3,$$
$$U_2=(z_\zeta r_\xi-z_\xi r_\zeta)u_1+r(\theta_\zeta z_\xi-\theta_\xi z_\zeta)u_2+r(r_\xi\theta_\xi-r_\xi\theta_\zeta)u_3,$$
$$U_3=(z_\xi r_\eta-z_\eta r_\xi)u_1+r(\theta_\xi z_\eta-\theta_\eta z_\xi)u_2+r(r_\xi\theta_\eta-r_\eta\theta_\xi)u_3 \quad (6)$$

and B_i^j represents the following product:

$$B_i^j=\beta_k^i\beta_k^j, \quad (7)$$

where

$$\beta_k^i=r_k\left(\mathrm{Cof}\frac{\partial z_i}{\partial\xi_k}\right). \quad (8)$$

The associated source terms for transports of the moment, temperature, k, and ε are given by Liu [2].

The equations were discretized using the finite volume method. The flow convection was approximated by second-order linear upwind differencing. The computational grids were arranged in a nonstaggered manner and the SIMPLEC method was used to deal with the coupling between the continuity and the momentum equations. It would lead to velocity–pressure decoupling and thus produce checkboard oscillations, and hence, the momentum interpolation method of Rhie and Chow [3] was employed to calculate the velocities across the cell faces. The physical plane velocity components were used as the solution variables, while the contravariant velocities were used as the cell face velocity variables [4] . Following the SIMPLEC algorithm, the face velocities were forced to satisfy the continuity constraint, and thus a pressure-correction equation was obtained. Because the serious nonorthogonality of grid lines may prevent the solution from converging, the full pressure-correction equation was solved without any simplification, as suggested by Chao and Chang [5] . Thus, the total number of points contained in the computational template was 19. The three-dimensional seven-pint strongly implicit procedure of Stone [6] was adopted as the basic iteration. Those corner-node contributions were absorbed in the source term and updated after each sweep of relaxation. The wall function theory and their applications in the nonorthogonal curvilinear coordinate system could be found in [7,8].

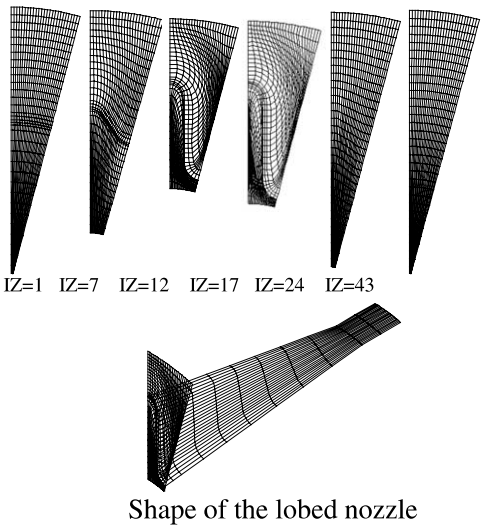

Fig. 6. Typical mesh used in the calculation.

Because of geometric periodicity and flow symmetry, only half a lobe of 15° was necessary in the calculations, as shown in Fig. 1. The computational grids are shown in Fig. 6, in which *IZ* represents the sequence of grid layer in the axial z direction. The serious grid skewness can be found in Fig. 6.

5. Simulated results and discussion

The numerical simulations were performed for the entire lobed nozzle mixer shown in Fig. 1. The mass flow rates on the primary and the secondary sides and the

Table 3
Tested and computational data

T_s, °C	T_p, °C	With plug		Without plug	
		m_p	m_s	m_p	m_s
25	25	0.3161	0.2684	0.4296	0.2164
25	175	0.2817	0.2755	0.4032	0.2313
25	250	0.2656	0.2755	0.3921	0.2415
25	345	0.2520	0.2739	0.3661	0.2473

flow temperature could be found in Table 3. The area ratio of mixer to the exit section of lobed nozzle was 3.08, and the secondary flow inlets were D100 and D80, with inlet velocity profiles assumed uniform. The turbulence was taken as about 2% of the inlet velocity for the primary flow and about 5% for the secondary flow. The length scale was chosen as an equivalent hydraulic diameter of the inlet cross-section. In order to prevent the disturbance of boundary condition to the exit flow of mixer, the computational zone was expanded to additional 27.8ς distance along the axial direction of the mixer.

5.1. Mixing processes between the primary and the secondary flow

Fig. 7 presents the velocity vector in sequential cross-sections of the mixer and the local magnification of streamwise vortex core with a central plug, the position of exit cross-section of lobed nozzle being defined as $Z = 0$. Comparing with Fig. 8 for without a central plug, the formation of streanwise vortex with a central plug is greatly prior to that without a central plug because the vortex is obvious in the position $Z/\lambda = 3.34$ with a central plug, while in $Z/\lambda = 7.03$ without a central plug, and the radial velocity component of secondary flow with a central plug is much greater than that without a central plug.

Figs. 9 and 10 present the contours of axial velocity component with and without a central plug, respectively.

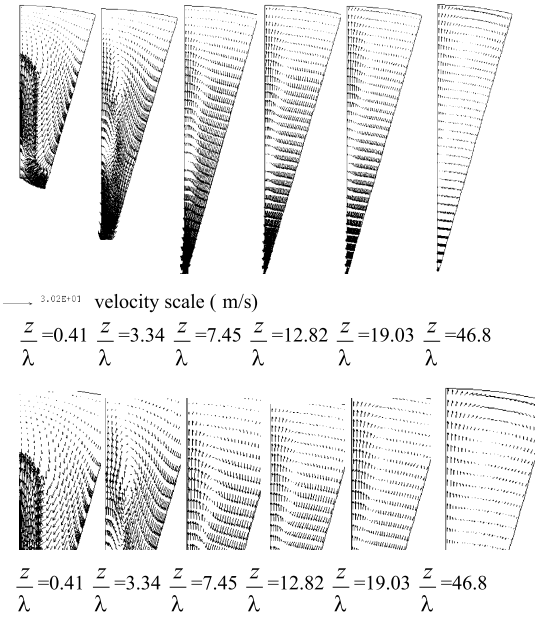

Fig. 7. The velocity vector and local magnification with central plug.

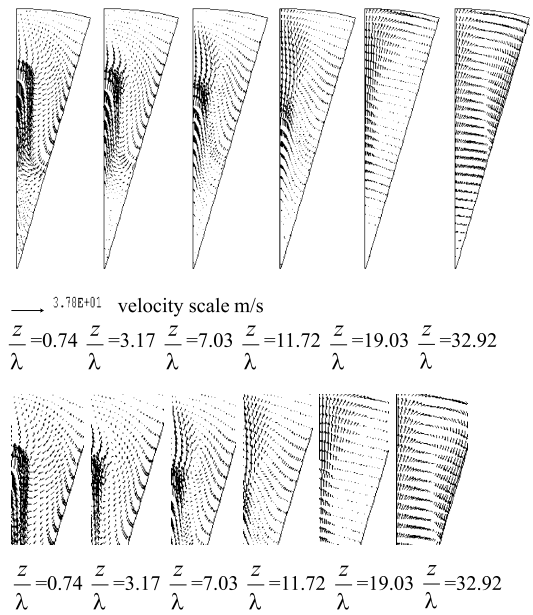

Fig. 8. The velocity vector and local magnification without central plug.

From both the figures, the contours in the exit position of lobed nozzle were the same as lobe shape. The contour lines in Fig. 9 become the radial ones gradually, while the contour lines in Fig. 10 become the vortex ones lastly.

5.2. Thermal mixing efficiency and temperature fields

In order to evaluate the thermal mixing state quantitatively, the thermal mixing efficiency was defined as [9]:

$$\eta = \frac{\int T^{0.5}\,\mathrm{d}m - T_{\mathrm{p}}^{0.5} m_{\mathrm{p}} - T_{\mathrm{s}}^{0.5} m_{\mathrm{s}}}{T_{\mathrm{mix}}^{0.5}(m_{\mathrm{p}} + m_{\mathrm{s}}) - T_{\mathrm{p}}^{0.5} m_{\mathrm{p}} - T_{\mathrm{s}}^{0.5} m_{\mathrm{s}}}. \tag{9}$$

For the cases that the temperatures of primary flow were 175, 250 and 345 °C, respectively, the secondary flow

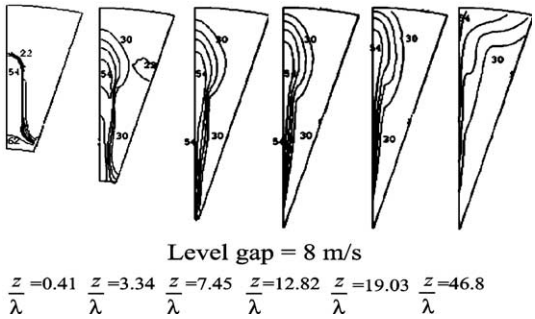

Fig. 9. Contour of the axial velocity (m/s), with central plug.

were 25 °C, and the total pressure prior to flow's entry into lobed nozzle were same, the calculated thermal mixing efficiencies based on the present numerical results vs the nondimensional axial distance are shown in Fig. 11, from which the central plug in the lobed nozzle plays an important role on promoting the thermal mixing between the primary and the secondary flows. In the side of mixer near to lobed nozzle, the increasing rate of thermal mixing with a central plug was much greater than that without a central plug. In the exit cross-section of mixer, the maximum thermal mixing efficiency with a central plug was 0.992%, 11.8% more than that without a central plug.

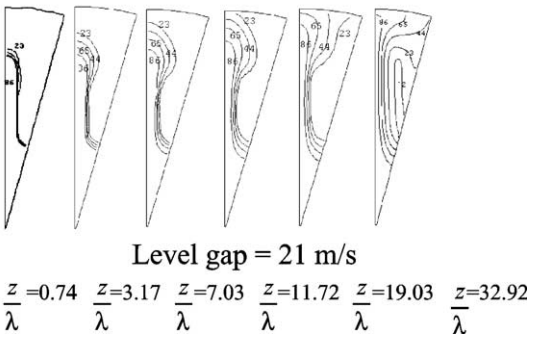

Fig. 10. Contour of the axial velocity (m/s), without central plug.

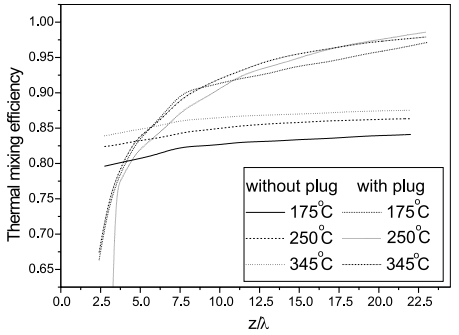

Fig. 11. Thermal mixing efficiencies vs nondimensional axial distance.

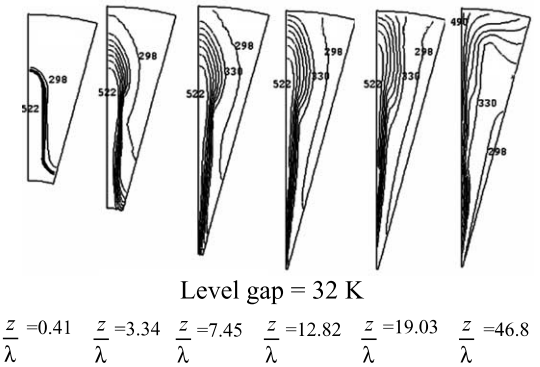

Fig. 12. Temperature contours (K), with central plug.

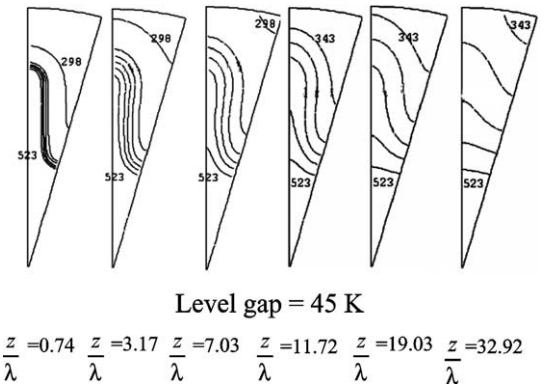

Fig. 13. Temperature contours (K), without central plug.

Table 4
Axial velocity profile in the exit cross-section of mixer

Y/R	W/W_{max}	
	Without plug	With plug
0.06	1.000	0.508
0.12	0.998	0.508
0.22	0.998	0.486
0.28	0.987	0.472
0.38	0.927	0.461
0.44	0.800	0.459
0.53	0.647	0.479
0.59	0.478	0.532
0.69	0.400	0.601
0.75	0.401	0.750
0.84	0.454	0.911
0.91	0.541	0.976
0.97	0.639	1.000

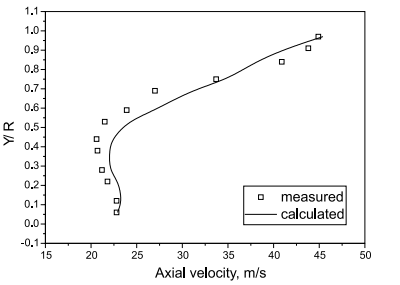

Fig. 14. The axial velocity profile with central plug.

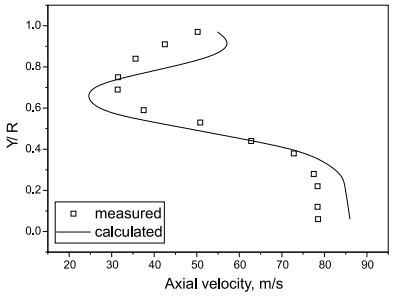

Fig. 15. The axial velocity profile without plug.

Figs. 12 and 13 present the temperature contours in a sequential cross-sections of mixer of axial direction, with and without a central plug, for the case of primary flow temperature being 250 °C and the secondary flow temperature being 25 °C. It can be seen from the Figs. 12 and 13 that although the inlet boundary conditions and the temperature contours in the exit section of lobed nozzle are same, the thermal mixing processes between the primary and the secondary flows for the cases of with and without a central plug are quite different. The temperature contour lines with a central plug gradually become radial lines after the thermal mixing between the primary and the secondary flows, while for without a central plug the temperature contour lines lastly become circumferential lines. It could also be seen from Fig. 13 that the central zone of the cylindrical mixer is always kept at elevated temperature state, which is wholly different from Fig. 12 that the low temperature contour lines could reach to the axis of the cylindrical mixer. That is the fundamental reason why the thermal mixing efficiency with a central plug is much more than that without a central plug.

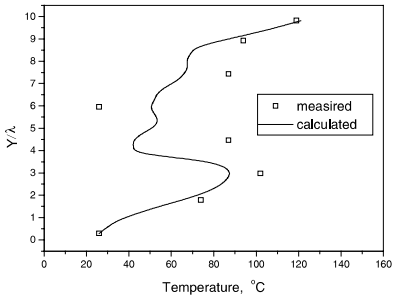

(a) $T_p = 175\,^{\circ}C$

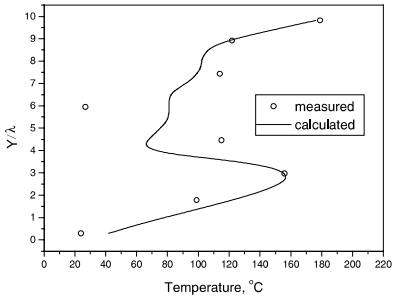

(b) $T_p = 250\,^{\circ}C$

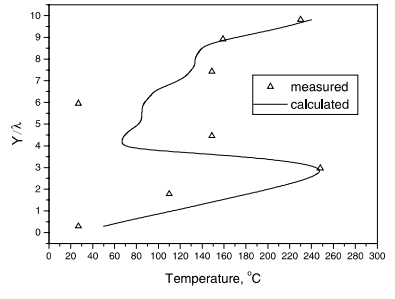

(c) $T_p = 345\,^{\circ}C$

Fig. 16. Temperature profiles with a central plug.

Table 5
Measured temperature profiles in the exit cross-section of the mixer

Y/R	T_p		
	175 °C	250 °C	345 °C
Without plug			
0.073	176	245	340
0.226	176	245	340
0.377	161	226	313
0.533	100	134	175
0.686	65	70	100
0.845	43	49	50
0.993	25	26	26
With plug			
0.073	26	26	27
0.226	74	99	110
0.377	102	156	248
0.533	87	115	149
0.686	26	27	27
0.845	87	114	149
0.993	119	179	230

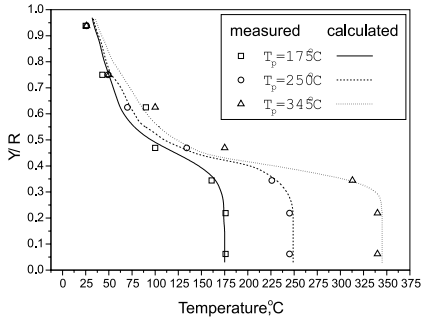

Fig. 17. Temperature profile without central plug.

5.3. Axial velocity and temperature profile in the exit section of the mixer

Table 4, Figs. 14 and 15 show the relative axial velocity, W/W_{max}, vs nondimensional radial distance in the exit section of cylindrical mixer along the radial line rotated 5° from the lobe peak position to the lobe bottom position, for the case that $\lambda = 3.08$ (without plug), and the secondary flow inlets are D100 and D80. In the figures, Y refers to the radial distance from the center of cylindrical mixer and R represents radius of the cylindrical mixer. Good agreements can be found in the center and the wall nearby, and the computational axial velocities are slightly higher than the measured ones in the shear mixing region. The axial velocity profile with a central plug is greatly different from that without a central plug, as shown in Figs. 14 and 15.

The temperature of mixing flow calculated and measured by temperature rakes in the exit section of the cylindrical mixer along the radial line of the lobe bottom position with and without a central plug vs nondimensional radial distance are shown in Table 5, Figs. 16 and 17, for the case that the area ratio $\lambda = 3.08$ (without central plug), the primary flow temperature is 175, 250 and 345 °C, respectively, and the secondary flow inlets are D100 and D80. There are good agreements in the center and the wall nearby, but noticeable differences between the computational and the measured ones in the shear-mixing region. The temperature profile with a central plug is greatly different from the one without a central plug, as shown in Figs. 16 and 17. The central plug strongly improved the mixing uniformity between the primary and the secondary flows.

6. Conclusions

By experiments and numerical simulations focused on the comparison of with and without a plug in the center of lobed nozzle, following conclusions can be made:

1. The central plug changes dramatically the mixing process between the primary and the secondary flows, and increases the pumping ratio by about 60%.
2. The central plug increases the total pressure prior to flow's entry into lobed nozzle by 0.8–1.0%, and hence increases the frictional loses of the primary flow.
3. The temperature-corrected parameters which make the modified pumping ratio get rid of the density or temperature effect, in the cases with and without a central plug, are same as 0.4.
4. According to the numerical simulations, in the guides of tilted wall surface of the central plug, the cool secondary flow can reach the core of the elevated primary flow in a very short axial distance of mixer, which makes a distinct difference from that, without a central plug the elevated primary flow prevents the cool secondary flow from convection into the center of the mixer. The different physical processes make the thermal mixing efficiency with a central plug be much higher than that without a central plug, and thus make the mixing between the primary and the secondary flows with a central plug more uniformly than that without a central plug.

Acknowledgements

The author would like to thank Prof. Li Li-Guo for extended support and to Mr. Chen Qiang for his assistance in performing partial experiment.

References

[1] M.W. Presz, R. Gousy, B. Morin, Forced mixer lobes in ejector designs, AIAA 86-1614, 1986.
[2] Y.H. Liu, Experimental and numerical investigation of lobed exhaust-ejector mixers at room and elevated temperature, Ph.D thesis, Nanjing University of Aeronautics and Astronautics, China, 2000.
[3] C.W. Rhie, W.L. Chow, A numerical study of the turbulent flow past an isolated airfoil with trailing edge separation, AIAA 82-0998, 1982.
[4] W. Shyy, T.C. Vu, On the adoption of velocity variable and grid system for fluid flow computation in curvilinear coordinates, J. Comput. Phys. 92 (1991) 82–105.
[5] M.J. Chao, M.K. Chang, New treatment of nonorthogonal terms in the pressure-correction equation, Numer. Heat Transfer B 26 (1994) 133–145.
[6] H.L. Stone, Iterative solution of implicit approximations of multidimensional partial differential equations, SIAM J. Numer. Anal. 5 (1968) 530–558.
[7] D.L. Sondak, Application of wall functions to generalized nonorthogonal curvilinear coordinate systems, AIAA J. 33 (1995) 33–41.
[8] P.G. Huang, Comment on application of wall functions to generalized nonorthogonal curvilinear coordinate systems, AIAA J. 33 (1995) 2445–2446.
[9] P. Koutmos, J.J. McGuirk, Turbofan forced mixer/nozzle temperature and flow field modeling, Int. J. Heat Mass Transfer 32 (1989) 1141–1153.